Received: 6 July 2020 | Revised: 18 September 2020 | Accepted: 28 January 2021

DOI: 10.1002/aoc.6203

FULL PAPER

Applied
Organometallic
Chemistry

WILEY

Liquid-phase oxidation of olefins with rare hydronium ion salt of dinuclear dioxido-vanadium(V) complexes and comparative catalytic studies with analogous copper complexes

Abhishek Maurya | **Chanchal Haldar**

Department of Chemistry, Indian Institute of Technology (Indian School of Mines), Dhanbad, Jharkhand, 826004, India

Correspondence
Chanchal Haldar, Department of Chemistry, Indian Institute of Technology (Indian School of Mines), Dhanbad 826004, Jharkhand, India.
Email: chanchal@iitism.ac.in

Funding information
Science and Engineering Research Board, Grant/Award Numbers: SB/EMEQ-055/2014, SB/FT/CS-027/2014

Homogeneous liquid-phase oxidation of a number of aromatic and aliphatic olefins was examined using dinuclear anionic vanadium dioxido complexes $[(VO_2)_2(^{sal}LH)]^-$ (**1**) and $[(VO_2)_2(^{Nsal}LH)]^-$ (**2**) and dinuclear copper complexes $[(CuCl)_2(^{sal}LH)]^-$ (**3**) and $[(CuCl)_2(^{Nsal}LH)]^-$ (**4**) (reaction of carbohydrazide with salicylaldehyde and 4-diethylamino salicylaldehyde afforded Schiff-base ligands $[^{sal}LH_4]$ and $[^{Nsal}LH_4]$, respectively). Anionic vanadium and copper complexes **1**, **2**, **3**, and **4** were isolated in the form of their hydronium ion salt, which is rare. The molecular structure of the hydronium ion salt of anionic dinuclear vanadium dioxido complex $[(VO_2)_2(^{sal}LH)]^-$ (**1**) was established through single-crystal X-ray analysis. The chemical and structural properties were studied using Fourier transform infrared (FT-IR), ultraviolet–visible (UV–Vis), ^{1}H and ^{13}C nuclear magnetic resonance (NMR), electrospray ionization mass spectrometry (ESI-MS), electron paramagnetic resonance (EPR) spectroscopy, and thermogravimetric analysis (TGA). In the presence of hydrogen peroxide, both dinuclear vanadium dioxido complexes were applied for the oxidation of a series of aromatic and aliphatic alkenes. High catalytic activity and efficiency were achieved using catalysts **1** and **2** in the oxidation of olefins. Alkenes with electron-donating groups make the oxidation processes easy. Thus, in general, aromatic olefins show better substrate conversion in comparison to the aliphatic olefins. Under optimized reaction conditions, both copper catalysts **3** and **4** fail to compete with the activity shown by their vanadium counterparts. Irrespective of olefins, metal (vanadium or copper) complexes of the ligand $[^{sal}LH_4]$ (**I**) show better substrate conversion(%) compared with the metal complexes of the ligand $[^{Nsal}LH_4]$ (**II**).

KEYWORDS

anionic vanadium complex, copper complex, homogeneous catalysis, hydronium ion salt, olefins oxidation

1 | INTRODUCTION

There is a constant demand for various value-added chemicals like alcohols, aldehydes, acids, esters, epoxides, etc. in both industrial and chemical industries,[1] and it is growing faster than ever. All these carbonyl compounds and alcohols are traditionally used as solvents, perfumes, and flavoring agents or essential intermediates for various chemical feedstocks, polymers, and agrochemicals. These carbonyl compound-based active intermediates are used as primary materials for the production of dyes, epoxy resins, paints, polymers, perfumes, pharmaceuticals, plastics, and surfactants.[2] Conventionally these carbonyl compounds are produced by the oxidation of olefins with the stoichiometric amount of conventional oxidizing agents like permanganates, peracids, hydrogen peroxides, or atmospheric O_2.[3,4] However, they often lead to low substrate conversion and the formation of undesirable side products. Thus, transition metal-based complexes appear like an alternative, green, and economical catalytic systems for the oxidation of olefins. A large number of the report is evolving in the literature dealing with the oxidation of olefins by various transition metal (such as Ti, V, Cr, Mn, Co, Ni, Cu, Mo, Ru, and Re) based catalysts in the presence of peroxides, peracids, and other oxidizing reagents.[5–7] Among all the transition metals mentioned above, vanadium and copper hold a unique and popular choice in the field of oxidation catalysts of various organic compounds.[8] Because of the high natural abundance and lower price, vanadium and copper complexes are considered to be the most effective and vital catalysts in the chemical industry. Moreover, they are found to be actively involved in catalyzing the alkene oxidation, epoxidation, sulfoxidation, alcohol oxidation, oxidative bromination, oxidative couplings, and condensations.[5b,6,9] Over the past decades, a vast number of vanadium and copper Schiff-base complexes have been synthesized and applied for the oxidation of various olefins.[2a,10]

However, the importance of the ligand environment is unquestionable to tune the catalytic efficiency of a catalyst. In this connection, Schiff-bases come across as being an effective and prime ligand system. The polydentate nature of the Schiff-bases allows them to create an impressive coordination sphere around the transition metal, which is suitable for various applications such as catalysis, chemical analysis, photophysical studies, biological research, and optics.[11] Also, Schiff-base complexes of transition metal generally improve the effectiveness of hydrogen peroxide by converting it into metal peroxides during the alkene oxidation. In the processes of catalytic oxidation of olefins, the effectiveness of a transition metal catalyst preferentially increases with the increasing oxidation state of the metal. There are several factors responsible for achieving the maximum oxidation state of the transition metal in their complexes. Those are (i) higher oxygen affinity, (ii) Lewis acid character of the transition metal, (iii) easy interconvertible oxidation states, and (iv) easy interchangeable coordination numbers.[12]

Higher oxygen affinity, variable valances, and coordination number make vanadium and copper complexes an ideal choice for designing an oxidation catalyst for the olefins. Hence, the proper design of a multidentate Schiff-base ligand, along with the proper choice of a transition metal, is the critical factor for the development of a productive and powerful oxidation catalyst. Based on the above discussion, it will be an interesting observation to compare the catalytic activity of vanadium and copper catalysts prepared by using the same Schiff-base ligands for the alkene oxidation, which may help us to identify the impact of metal centers on the catalytic reaction.

Hence, in the current article, we have prepared two hexadentate Schiff-base ligands $[^{sal}LH_4]$ (**I**) and $[^{Nsal}LH_4]$ (**II**) with N and O donor atoms, by reacting carbohydrazide with salicylaldehyde and 4-diethylamino salicylaldehyde, respectively. The hexadentate Schiff-bases were chosen in such a way that each ligand can accommodate two metal centers simultaneously without involving any extra bridging group/atoms in between the metal centers. The restricted electronic distribution between the two metal atoms of the same complex can allow the individual metal atom to function as an independent catalytic center. Herein, we report four binuclear metal complexes $[H_3O][(VO_2)_2(^{sal}LH)]$ (**1**), $[H_3O][(VO_2)_2(^{Nsal}LH)]$ (**2**), $[H_3O][(CuCl)_2(^{sal}LH)]$ (**3**), and $[H_3O][(CuCl)_2(^{Nsal}LH)]$ (**4**), which were synthesized by reacting $[^{sal}LH_4]$ (**I**) and $[^{Nsal}LH_4]$ (**II**) with the metal precursors of vanadium and copper. The ligand $[^{sal}LH_4]$ (**I**) and its vanadium complex $[NH_4][(VO_2)_2(^{sal}LH)]$ (**1**) can be found in earlier literature.[13] However, here, we were able to crystallize complex **1** in the form of its hydronium ion salt with 2 eq. of DMF as the solvent of crystallization. First time we are introducing the vanadium and copper complexes $[H_3O][(VO_2)_2(^{Nsal}LH)]$ (**2**), $[H_3O][(CuCl)_2(^{sal}LH)]$ (**3**) and $[H_3O][(CuCl)_2(^{Nsal}LH)]$ (**4**). All the prepared vanadium and copper complexes successfully catalyzed the oxidation of a range of alkenes in the presence of hydrogen peroxide, a green oxidant. However, vanadium complexes show their superior behavior over copper-based catalysts for the alkene oxidation.

2 | EXPERIMENTAL

2.1 | Materials

Salicylaldehyde (SRL, India), 4-diethylamino salicylaldehyde (Alfa-Aesar, India), carbohydrazide (TCI, Japan), $CuCl_2.2H_2O$ (Loba Chemie, India), V_2O_5 (Merck, India), acetylacetone (Merck, India), sulphuric acid (Merck, India), potassium carbonate (Merck, India), 30% H_2O_2 (Merck, India), 70% TBHP (Merck, India), styrene (Alfa-Aesar, India), allylbenzene (Alfa-Aesar, India), 1-methyl cyclohexene (Alfa-Aesar, India), *cis*-cyclooctene (Alfa-Aesar, India), 1-octene (Alfa-Aesar, India), 4-chlorostyrene (TCI, Japan), indene (TCI, Japan), 2-norbornene (TCI, Japan), limonene (TCI, Japan), divinylbenzene (TCI, Japan), and AR grade solvents (Merck & Rankem, India) were used as received. HPLC grade methanol (Spectrochem, India), *n*-hexane (Spectrochem, India), and acetonitrile (Spectrochem, India) were used as received for GC analysis. $VO(acac)_2$ was prepared by following the reported method.[14]

2.2 | Physical methods and analysis

The structure of ligands and metal complexes was characterized by various physicochemical methods. Fourier transform infrared (FT-IR) (4,000–400 cm^{-1}) spectra of ligands and metal complexes were recorded on an Agilent Cary 600 Series FT-IR Spectrometers by the ATR method. ^1H nuclear magnetic resonance (NMR) and ^{13}C NMR spectra of the ligands were recorded in DMSO-d_6 solvent on a Bruker Avance II 400 MHz NMR spectrometer with the general parameter settings. Electronic spectra of ligands and metal complexes were recorded in a “SHIMADZU” UV-1800 spectrophotometer using DMF/methanol. The electrospray ionization mass spectrometry (ESI-MS) of the metal complexes were analyzed by Waters Q-Tof Micromass. Thermogravimetric analysis (TGA) and differential thermal analysis (DTA) were performed by using Perkin Elmer, Diamond TG/DTA instrument. The X-band electron paramagnetic resonance (EPR) measurements of copper complexes were performed in a JES-FA200 ESR spectrometer. Catalytic oxidation of various alkenes was monitored by an Agilent 7890B gas-chromatograph fitted with an HP-5 capillary column (30 m × 0.25 mm × 0.25 μm) and an flame ionization detector (FID). The products of the catalytic reaction were identified by Thermo GC–MS (Trace 1300 ISQ QD) with a TG-5MS capillary column (30 m × 0.25 mm × 0.25 μm) and a mass detector.

2.3 | X-ray crystallography

The single-crystal X-ray data of complex $[H_3O][(VO_2)_2(^{sal}LH)].2(CH_3)_2NCH$ (**1**) was collected by Rigaku Oxford Diffraction system equipped with state of the art CCD Eos S2 detector using MoK_α radiation (wavelength 0.71073 Å) at room temperature. The structure was solved by direct methods using SIR-2004[15] and refined on F^2 by full-matrix least square method using SHELXL-2018.[16] The nonhydrogen atoms (C, O, N, and V) were refined anisotropically, and hydrogen atoms were included in the refinement on calculated positions riding on their carrier atoms. The molecular graphics were haggard using the PLATON program. The function minimized was $[\Sigma w\ (F_o^2 - F_c^2)^2]$ $(w = 1/[\sigma^2(F_o^2) + (aP)^2 + bP])$, where $P = (\mathrm{Max}\ (F_o^2,0) + 2F_c^2)/3$ with $\sigma^2(F_o^2)$ from counting statistics. The function R_1 and wR_2 were $(\sigma||F_o| - |F_c||)/\sigma|F_o|$ and $[\sigma w\ (F_o^2 - F_c^2)^2/\sigma (wF_o^4)]^{1/2}$, respectively. CCDC No. 2009184 carries the supplementary crystallographic data of complex **1** for this paper. Detailed crystallographic data are enlisted in Tables 1 and S1.

3 | PREPARATIONS

3.1 | Synthesis of hexadentate Schiff-bases $[^{sal}LH_4]$ (I) and $[^{Nsal}LH_4]$ (II)

Ligands (**I**) and (**II**) were prepared by adopting the methods reported in the literature[17] and presented in Scheme 1. Briefly, the methanolic solution of (10 ml) carbohydrazide (0.90 g, 0.01 mol) was reacted with salicylaldehyde (2.44 g, 0.02 mol) or 4-diethylamino salicylaldehyde (3.86 g, 0.02 mol) under the refluxing condition for 5–6 h. The volume of the resulting reaction mixture was reduced to ~5 ml. After keeping the solution at room temperature, the white-colored precipitate was separated and washed with cold methanol followed by petroleum ether and dried under vacuum over silica gel.

3.1.1 | Data for $[^{sal}LH_4]$ (I)

Yield: 62.78%; Anal. Calcd. For $C_{15}H_{14}N_4O_3$ (MW 298.30); C, 60.40%; H, 4.73%; N, 18.78%; found: C, 60.53%; H, 4.81%; N, 18.65%; FT-IR (ATR, cm^{-1}): 3,413 (ν_{O-H}), 3,254 (ν_{N-H}), 1,708 ($\nu_{C=O}$), 1,609($\nu_{C=N}$); ultraviolet–visible (UV–Vis) [λ_{max} (nm), ε ($L\ mol^{-1}\ cm^{-1}$)]: 231 (3.46×10^3), 250 (Sh) (2.89×10^3), 341 (Sh) (2.02×10^3), 384 (2.84×10^3), 454 (3.28×10^3); ^1H NMR (DMSO-d_6, δ in ppm): 6.8–6.8 (m, 4H), 7.1–7.2

TABLE 1 Crystal and refinement parameters for complex $[H_3O][(VO_2)_2(^{sal}LH)].2(CH_3)_2NCH$ (**1**).

Identification code	**(1)**
Empirical formula	$C_{21}H_{28}N_6O_{10}V_2$
Formula weight	626.37
Temperature/K	293 (2)
Crystal system	Triclinic
Space group	P-1
a (Å)	9.2398 (16)
b (Å)	11.2699 (14)
c (Å)	13.584 (2)
α (°)	89.473 (11)
β (°)	74.417 (14)
γ (°)	76.228 (13)
Volume (Å^3)	1,321.1 (4)
Z	2
ρcalc (g cm^{-3})	1.575
μ (mm^{-1})	0.772
F(000)	644.0
Radiation Mo Kα (λ)	0.71073
2θ range for data collection (°)	3.728 to 51.994
Index ranges	$-11 \leq h \leq 10$, $-13 \leq k \leq 13$, $-13 \leq l \leq 16$
Reflections collected	9,948
Independent reflections	5,069 ($R_{int} = 0.1411$, $R_{sigma} = 0.2025$)
Data/restraints/ parameters	5,069/0/368
Goodness of fit on F^2	0.930
Final R indexes $R_1(I > 2\sigma(I))$, wR_2	$R_1 = 0.1040$, $wR_2 = 0.2120$
Final R indexes (all data) R_1, wR_2	$R_1 = 0.1896$, $wR_2 = 0.2554$
Largest diff. peak/hole/e Å^{-3}	0.95/−0.63

(m, 2H), 7.6 (s, 2H), 8.3 (s, 2H), 10.5 (s, 2H), 10.8 (s, 2H); ^{13}C NMR (DMSO-d_6, δ in ppm): 116.2, 119.2, 119.7, 128.1, 130.7, 147.2, 152.0, 156.6.

3.1.2 | Data for $[^{Nsal}LH_4]$ (II)

Yield: 72.45%; Anal. Calcd. For $C_{23}H_{32}N_6O_3$ (MW 440.54); C, 62.71%; H, 7.32%; N, 19.08%; found: C, 62.43%; H, 7.53%; N, 18.94%; FT-IR (ATR, cm^{-1}): 3,398 (ν_{O-H}), 3,260 (ν_{N-H}), 1,699 ($\nu_{C=O}$), 1,627 ($\nu_{C=N}$); UV–Vis [λ_{max} (nm), ε (L mol^{-1} cm^{-1})]: 218 (2.95 × 10^3), 249 (1.43 × 10^3), 337 (Sh) (4.48 × 10^3), 367 (7.32 × 10^3); ^{1}H NMR (DMSO-d_6, δ in ppm): 1.0–1.1 (t, 12H), 3.2–3.3 (q, 8H), 6.1–6.1 (m, 2H), 6.2–6.2 (m, 2H), 7.3–7.3 (m, 2H), 8.2 (s, 2H), 10.3 (s, 2H), 10.6 (s, 2H); ^{13}C NMR (DMSO-d_6, δ in ppm): 12.5, 43.8, 97.6, 103.6, 107.4, 130.1, 144.4, 149.6, 152.1, 158.5.

3.2 | Synthesis of $[H_3O][(VO_2)_2(^{sal}LH)]$ (1) and $[H_3O][(VO_2)_2(^{Nsal}LH)]$ (2)

A common route was followed for the preparation of the complexes **1** and **2**. Briefly, a methanolic solution of $[VO(acac)_2]$ (5.30 g, 0.02 mol) was reacted with methanolic solution of $[^{sal}LH_4]$ (**I**) (2.98 g, 0.01 mol) or $[^{Nsal}LH_4]$ (**II**) (4.40 g, 0.01 mol) under refluxing condition for 2 h. The resultant reaction mixture was kept for slow evaporation overnight. During this time, a green-colored precipitate of **1** and an orange-colored precipitate of **2** separated out from the reaction mixture. It was filtered, washed with hot methanol followed by petroleum ether, and dried in a vacuum under silica gel. Crude samples of **1** and **2** were dissolved in the mixed solvents (DMF and MeOH) and kept for crystallization. Within 6–7 days, yellowish colored crystals of **1**, suitable for single-crystal X-ray analysis, were filtered off, washed with cold methanol, and dried in air. Despite our continuing efforts, we were unable to get the crystals of **2** suitable for single-crystal X-ray analysis.

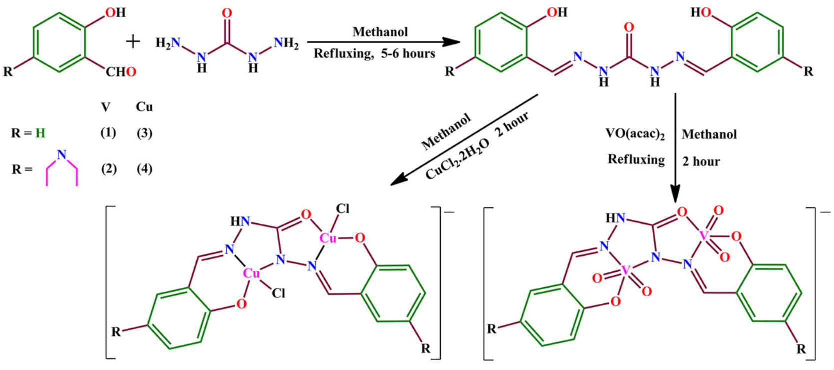

SCHEME 1 Synthetic scheme for the preparation of ligands $[^{sal}LH_4]$ (**I**) and $[^{Nsal}LH_4]$ (**II**) along with their corresponding vanadium (**1**–**2**) and copper (**3**–**4**) complexes

3.2.1 | Data for $[H_3O][(VO_2)_2(^{sal}LH)]$ (1)

Yield: 55.20%; Anal. Calcd. For $C_{15}H_{14}N_4O_8V_2$ (MW 480.18): C, 37.52%; H, 2.94%; N, 11.67%; found: C, 37.93%; H, 2.85%; N, 11.02%; FT-IR (ATR, cm^{-1}): 3,347 (ν_{O-H}), 3,212 (ν_{N-H}), 1,675 ($\nu_{C=O}$), 1,591 ($\nu_{C=N}$), 914, 932 ($\nu_{V=O}$); UV–Vis [λ_{max} (nm), ε (L mol^{-1} cm^{-1})]: 242 (1.71×10^3), 367 (1.38×10^3), 439 (9.62×10^2), 525 (5.05×10^2); electrospray ionization mass spectrometry (ESI-MS): m/z 461.93 (shown in Figure S13, calculate for $[(VO_2)_2(^{sal}LH)]^- = 461.15$).

3.2.2 | Data for $[H_3O][(VO_2)_2(^{Nsal}LH)]$ (2)

Yield: 58.01%; Anal. Calcd. $C_{23}H_{32}N_6O_8V_2$ (MW 622.42); C, 44.38%; H, 5.18%; N, 13.50%; found: C, 45.04%; H, 5.25%; N, 13.72%; FT-IR (ATR, cm^{-1}): 3,371 (ν_{O-H}), 3,203 (ν_{N-H}), 1,675 ($\nu_{C=O}$), 1,585 ($\nu_{C=N}$), 908, 944 ($\nu_{V=O}$); UV–Vis [λ_{max} (nm), ε (L mol^{-1} cm^{-1})]: 214 (6.18×10^3), 348 (4.09×10^3), 411 (2.81×10^3); ESI-MS: m/z 603.11 (shown in Figure S14, calculate for $[(VO_2)_2(^{Nsal}LH)]^- = 603.40$).

3.3 | Synthesis of $[H_3O][(CuCl)_2(^{sal}LH)]$ (3) and $[H_3O][(CuCl)_2(^{Nsal}LH)]$ (4)

By adopting similar methods as described earlier for the preparation of vanadium complexes **1** and **2**, we have prepared complexes **3** and **4**. Briefly, a methanolic solution of $CuCl_2.2H_2O$ (3.40 g, 0.02 mol) was mixed with a methanolic solution of $[^{sal}LH_4]$ (**I**) or $[^{Nsal}LH_4]$ (**II**) in 2:1 ratio with constant stirring under the refluxing condition for 2 h. The resultant reaction mixture was cooled and kept in a refrigerator overnight. Within a day, a greenish colored precipitate of **3** and **4** was filtered off, washed with cold methanol, and dried in a vacuum under silica gel.

3.3.1 | Data for $[H_3O][(CuCl)_2(^{sal}LH)]$ (3)

Yield: 68.78%; MW 512.29 ($C_{15}H_{14}Cl_2Cu_2N_4O_4$), FT-IR (ATR, cm^{-1}): 3,392 (ν_{O-H}), 3,209 (ν_{N-H}), 1,675 ($\nu_{C=O}$), 1,600 ($\nu_{C=N}$); UV–Vis [λ_{max} (nm), ε (L mol^{-1} cm^{-1})]: 222 (2.64×10^3), 276 (1.66×10^3), 392 (8.96×10^2), 639 (70.21); ESI-MS: m/z = 423.03 (shown in Figure S15, calculated $\{[(Cu_2(^{sal}LH)] + H\} = 423.36$).

3.3.2 | Data for $[H_3O][(CuCl)_2(^{Nsal}LH)]$ (4)

Yield: 55.98%; MW 654.54 ($C_{23}H_{32}Cl_2Cu_2N_6O_4$), FT-IR (ATR, cm^{-1}): 3,338 (ν_{O-H}), 3,197 (ν_{N-H}), 1,660 ($\nu_{C=O}$), 1,600 ($\nu_{C=N}$); UV–Vis [λ_{max} (nm), ε(L mol^{-1} cm^{-1})]: 213 (1.63×10^3), 224 (1.64×10^3), 238 (1.14×10^2), 296 (1.45×10^2), 308 (1.21×10^2), 661 (143); ESI-MS: m/z = 735.05 (calculated $\{[(CuCl)_2(^{Nsal}LH)].2H_2O.2MeOH\} = 735.63$); m/z = 601.24 (shown in Figure S16, calculated $[\{[Cu_2(^{Nsal}LH)].2H_2O\} + H] = 601.64$).

3.4 | Catalytic oxidation of alkenes

The catalytic efficiency of all the synthesized complexes **1**, **2**, **3**, and **4** were evaluated towards the catalytic oxidation of alkenes. All the reactions were performed in a 50-ml round-bottom flask fitted with a water-cooled condenser. In a typical reaction, styrene (0.520 g, 5 mmol) was reacted with 30% H_2O_2 (1.133 g, 10 mmol) in the presence of 0.003 g of catalyst precursor in 5 ml of MeOH with continuous stirring at 70°C of bath temperature for 6 h. A small portion of the reaction mixture was withdrawn periodically and extracted with *n*-hexane and analyzed by GC. The substrate conversion(%) and product selectivity(%) were calculated by using Equations 1 and 2. To find out the maximum substrate conversion(%) and product selectivity(%), reaction conditions were optimized by changing various parameters, that is, catalyst amount, oxidant amount, solvent amount, solvent nature, nature of oxidant, and reaction temperature.

$$\%\text{Conversion of Substrate} - 100 - \frac{\textit{Area of substrate}}{\textit{Total area of substrate} + \textit{Area of products}} \times 100, \tag{1}$$

$$\text{Similarly, } \%\text{Selectivity} = 100 - \frac{\textit{Area of product}}{\textit{Total area of products}} \times 100. \tag{2}$$

4 | RESULTS AND DISCUSSION

4.1 | X-ray crystallography

The molecular structure of the complex $[H_3O][(VO_2)_2(^{sal}LH)].2(CH_3)_2NCH$ (**1**) has been confirmed by single-crystal X-ray diffraction (XRD) analysis. The single crystals of **1** are quite sensitive to moisture. If kept for a long time in the air at room temperature, they start to lose their crystallinity and convert into powder, probably by losing the solvent of crystallization. The complex **1** crystalized in the triclinic crystal system with P-1 space group where each vanadium adopts distorted square pyramidal geometry. The ORTEP plot of **1** is displayed in Figure 1.

The asymmetric unit of the crystal structure of the molecule **1** carries an anionic binuclear vanadium complex with two molecules of DMF (solvent of crystallization) and one hydronium ion as a counter cation. A limited number of reports are available in the literature where hydronium ion was incorporated in the molecule to balance the charges.[18a,b]

Trianionic hexadentate carbohydrazide Schiff-base ligand ($H^{sal}L^{3-}$) captures two vanadium centers with a mutual distance of 5.007 Å, where each vanadium center is present as *cis*-dioxido form. Interestingly, both *cis*-VO_2 unit of each molecule is mutually *trans*-directed to each other (Figure 1b). The geometrical index τ is 0.23 for **1**, which ($\tau = 0$ for ideal square pyramidal and $\tau = 1$ for perfect trigonal bipyramidal geometry) describes the extent of distortion in the geometry around the metal centers.[18c] Interestingly, the electronic environment around both vanadium centers is not similar. The basal plane around the V1 is occupied by oxygen (O1) of phenolate group, azomethine nitrogen (N1) atom, and nitrogen (N3) from the carbohydrazide group, whereas V2 is surrounded by phenolate oxygen (O4), azomethine nitrogen (N4), and carbonyl oxygen (O5) of carbohydrazide group. The C8—O5 bond length is 1.264 Å, which is a little longer than the >C═O double bond length but significantly shorter than the C—O single bond indicating that the O5 is a carbonyl —O atom. The important bond angles and bond lengths of **1** are tabulated in Table S1.

Molecular association in the solid state of **1** is controlled by a number of weak interactions, dominated by strong and directional intermolecular H-bonding (Figure 2). One of the dioxido vanadium(V) oxygen involves in the intermolecular hydrogen bonding with the amine hydrogen of the neighboring molecule and vice versa (D—H .... A = 2.936 Å). A detailed list of H-bond distances is tabulated in Table S2. Each delicate hydronium ion is holding two O atoms from two DMF solvent molecules, one dioxido vanadium(V) oxygen, and one phenolate oxygen atom through H-bonding. These H-bondings are sufficiently strong enough to hold and stabilized the hydronium ion inside the crystal packing of **1**. Also, a weak interaction can be observed between one of the hydronium ion hydrogen and the neighboring dioxido vanadium(V) complex (Figure 2b).

4.2 | Spectroscopic analysis

A range of spectroscopic techniques was utilized to understand as well as establish the molecular structure of the prepared ligands and corresponding metal (vanadium and copper) complexes.

FT-IR spectroscopy was used to record the changes in functional groups in every step of the metal complex synthesis, starting from their respective ligands systems (**I**) and (**II**). Ligands (**I**) and (**II**) carry an FT-IR signal at 1,609 and 1,627 cm$^{-1,}$ respectively, which is the characteristic bands of $\nu_{C=N}$, suggesting the successful formation of the ligand systems. A sharp and strong stretching band due to $\nu_{C=O}$ appears at 1,708 (**I**) and 1,699 (**II**), cm^{-1}, which implies the existence of the ligands in the keto-form in the solid state. Additionally, both ligands display a broad signal for ν_{O-H} in the range of 3,398–3,413 cm^{-1} and ν_{N-H} in the range of 3,254–3,260 cm^{-1}. The FT-IR spectra of ligands and their metal complexes are displayed in Figures S1–S6. Selected stretching frequencies are tabulated in Table S3. Vanadium complexes **1** and **2** produce a couple of splitted

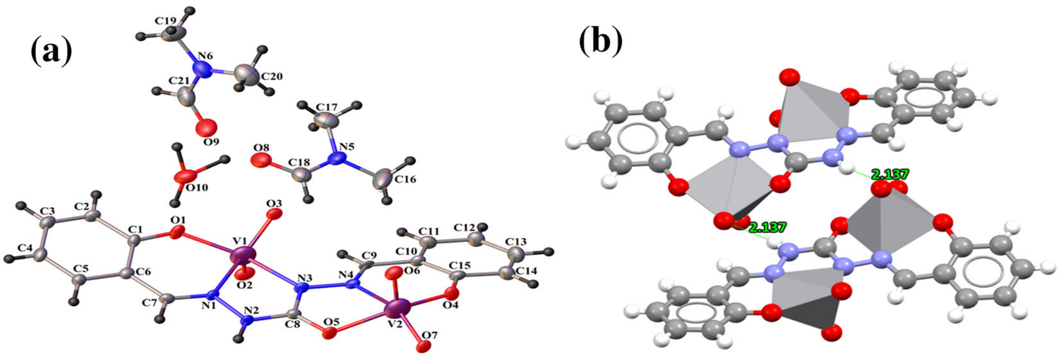

FIGURE 1 (a) ORTEP plot of the asymmetric unit in the crystal of complex $[H_3O][(VO_2)_2(^{sal}LH)].2(CH_3)_2NCH$ (**1**) with 50% thermal ellipsoids and (b) polyhedral plot of **1**

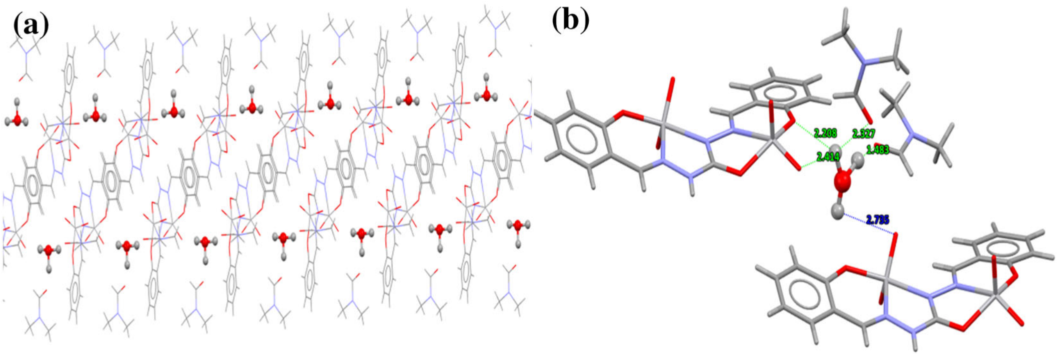

FIGURE 2 (a) Crystal packing **1** in a 3D structure in solid state and (b) intermolecular H-bonding involving hydronium $[H_3O]^+$ ion

vibrational band characteristics of ν_{sym}(O═V═O) and ν_{asym}(O═V═O) of $V^{(V)}O_2$ species, in the range of 914–932 cm^{-1} and 908–944 cm^{-1}, respectively.[5a,19] In both copper complexes **3** and **4**, stretching bands of $\nu_{C=O}$ and $\nu_{C=N}$ appear a little shifted towards the lower wavenumber compared with their corresponding ligand, which suggests the coordination of "O" of keto group and "N" atom of azomethine group to the copper center.[5a]

Successful metalation of the ligands $[^{sal}LH_4]$ (**I**) and $[^{Nsal}LH_4]$ (**II**) were further supported by the electronic spectroscopic analysis. UV–Vis spectra of ligands and their corresponding metal complexes were recorded in methanol and displayed in Figure S7. All the four metal complexes **1–4** show comparable electronic spectra with that of the free ligands. The vanadium complexes **1** and **2** exhibit an additional band in the range of 390–411 nm, which is assigned to phenolate "O" to vanadium(V) charge transfer transition. On the other hand, both copper complexes **3** and **4** displayed one low-intensity broad band in the range of 639–661 nm, characteristic of the *d*-*d* transition of Cu^{2+} center.[2c,20] The above-mentioned changes in the absorbance spectra of the metal complexes support the successful complexation. A list of important λ_{max} values along with the molar extinction coefficients (ε) are tabulated in Table S4. The gradual addition of a 2-drop portion of 0.1 M 30% H_2O_2 solution into a methanolic solution of **3** (3.67×10^{-4} M) and **4** (5.60×10^{-4} M) causes the disappearance of 639 nm (**3**) and 661 nm (**4**) bands respectively (shown in Figures 3 and S8), suggesting the conversion of Cu^{2+} into Cu^{3+} species in solution.

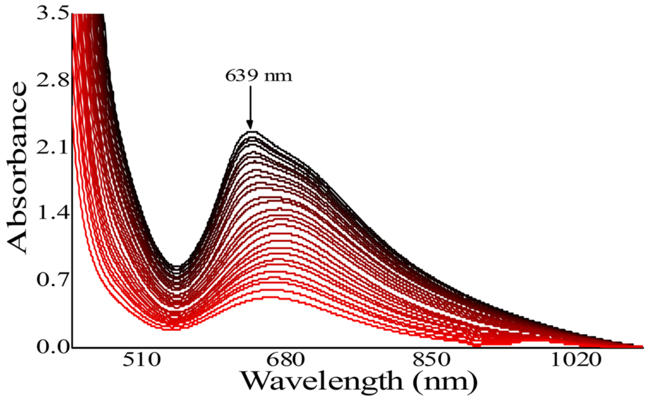

FIGURE 3 Spectral changes recorded by the gradual addition of two drops of 0.1M H_2O_2 solution in the 3.22×10^{-2} M DMSO solution of $[(CuCl)_2(^{sal}LH)]^-$ (**3**)

After getting the initial assessment from the FT-IR and UV–Vis spectroscopy, the molecular structure of the ligands $[^{sal}LH_4]$ (**I**) and $[^{Nsal}LH_4]$ (**II**) was confirmed through NMR spectroscopy. The proton NMR spectra of the ligands $[^{sal}LH_4]$ (**I**) and $[^{Nsal}LH_4]$ (**II**) are displayed in Figure 4, and the appropriate assignment of proton signals is given in Table S5. Ligand $[^{sal}LH_4]$ (**I**) shows the three aromatic proton signals of eight equivalent protons in the range of 6.8–7.2 ppm. A similar spectral pattern can be seen in the proton NMR spectra of the ligand (**II**) in the range of 6.1–7.3 ppm. Both ligands display a sharp singlet characteristic of azomethine proton at 8.3 (**I**) and 8.2 ppm (**II**). As expected, no aliphatic proton signal is visible in the ligand (**I**). A sharp triplet with 12 equivalent protons centered at 1.0 ppm due to the methyl (—CH_3, *J* = 6.9 Hz) groups and a quartet with 8 equivalent protons centered at 3.3 ppm, because of a methylene group (—CH_2—, *J* = 6.68, 6.88 Hz), can be seen in the ^1H NMR spectra of (**II**). Ligand (**I**) exhibits the characteristic —NH, and —OH proton signal at 10.5 and 10.8 ppm, respectively. As both the signals partially merge, the sharper signal is assigned to the less labile amine protons, whereas the broader signal is due to the labile —OH protons. Comparable spectra can be observed in the ligand (**II**), but alcoholic (—OH) protons appear more deshielded than the amine protons, which may be due to the stronger intramolecular H-bonding. ^1H NMR spectra of both ligands (**I**) and (**II**) were re-recorded in the presence of D_2O. Comparative analysis of ^1H-NMR spectra of (**I**) and (**II**) recorded in the presence of D_2O and without

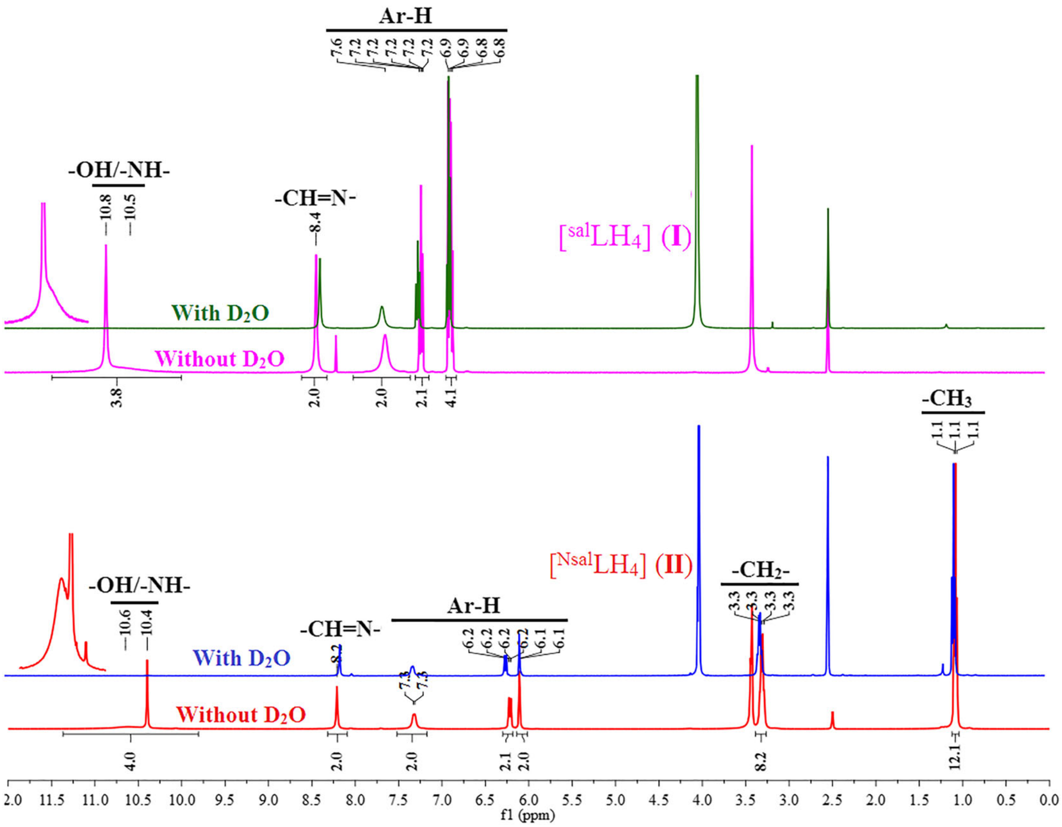

FIGURE 4 Comparative proton NMR spectra of ligands [^{sal}LH$_4$] (**I**) and [^{Nsal}LH$_4$] (**II**) recorded in DMSO-d_6 and in DMSO-d_6 + D_2O

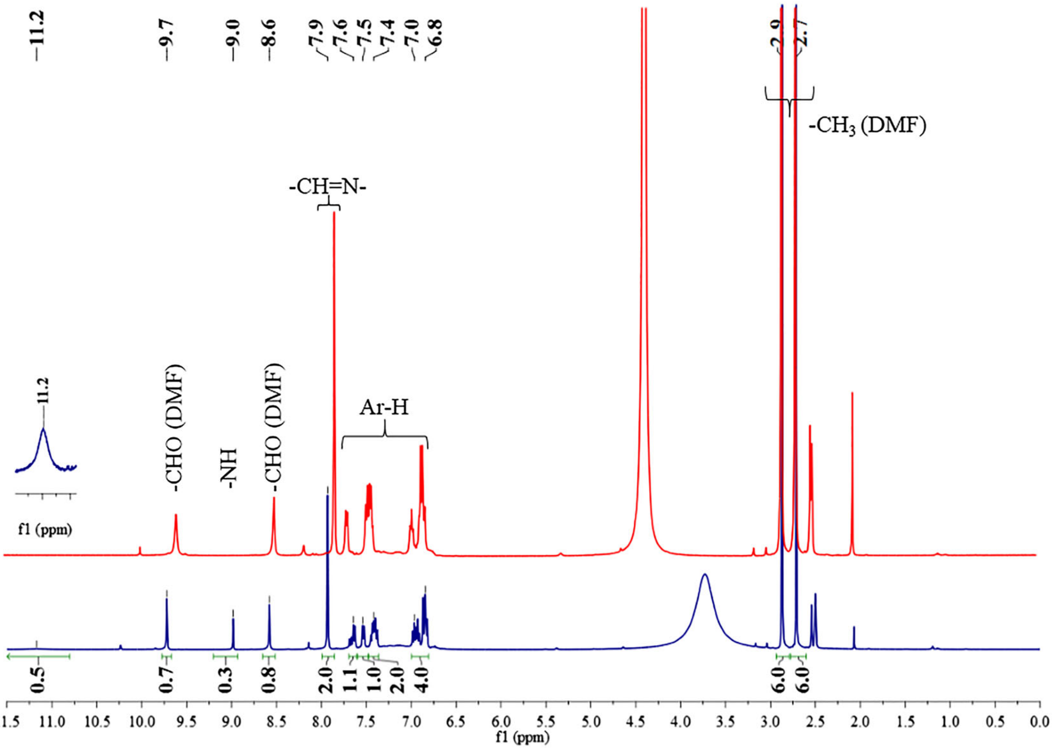

FIGURE 5 Comparative proton NMR spectra of **1** recorded in the presence and absence of D_2O using DMSO-d_6 as a base solvent

D_2O showed that in the presence of D_2O, proposed alcoholic (—OH) and amine (—NH) signals disappear along with slight shifting in the signals of aromatic and aliphatic protons. The absence of proton signals in the range of 10.3–10.8 ppm further confirms the —OH and —NH protons.

In the ^1H NMR spectrum of **1** (as shown in Figure 5), the signals due to the eight aromatic protons appear in the range of 6.8–7.6 ppm. A sharp singlet equivalent to two protons, due to the azomethine protons (—HC═N), is present at 7.9 ppm. A singlet because of one amine proton (—NH) is found at 9.0 ppm. Due to the presence of two molecules of DMF as solvent of crystallization in **1**, we observed two singlets in the range of 8.6–9.7 ppm arising from the aldehydic protons. Additionally, two singlets, equivalent to six protons each in the range of 2.7–2.8 ppm, were also observed due to the methyl groups of DMF molecules. A broad singlet at 11.2 ppm can also be seen due to the —OH of hydronium ion. The chemical shift of amine proton was determined by re-recording ^1H NMR spectrum of the DMSO-d_6 solution of **1** after adding a few drops of D_2O and compared with the original ^1H NMR spectrum (recorded in the presence of DMSO-d_6 only). Figure 5 shows that the addition of D_2O causes the disappearance of the 9.0- and 11.2-ppm signal, which confirms that the signals at 9.0 and 11.2 ppm are due to the —NH and —OH proton, respectively. The aromatic and aliphatic signals show slight shifting from their original chemical shift values. The —NH proton was further confirmed through ^1H—^1H COSY, and the spectrum is shown in Figure S9. All the diagonal peaks resemble what we observed in the ^1H NMR spectra of **1**. Two very weak cross-peaks appear at {7.9, 8.8} and {7.9, 6.8} ppm due to the magnetic interaction of one of the azomethine protons with amine and phenylic protons, respectively. These observations confirm the presence of —NH proton in **1**, and the chemical shift suggests that this amine group is not coordinated to the metal center.

The molecular frame of ligands [$^{sal}LH_4$] (**I**) and [$^{Nsal}LH_4$] (**II**) was further established by ^{13}C NMR spectra and is shown in Figure 6. The appropriate assignment of signals is tabulated in Table S6. Due to the symmetrical molecular arrangements, ^{13}C NMR spectra of ligands (**I**) and (**II**) show eight and ten non-equivalent carbon signals, respectively. The characteristic carbonyl carbon appears in (**I**) at 156.6 ppm, whereas (**II**) displays it at 158.5 ppm. Azomethine carbon signal appears at 147.2 (in **I**) and 149.6 ppm (in **II**). Except for the phenolic carbon atom, all the other aromatic carbon signals appear in their expected region. Additionally, ligand (**II**) exhibits two aliphatic carbon signals, one at 12.5 ppm, due to the —CH_3 groups, another at 43.8 ppm, because of the —CH_2— groups. All signals are in accordance with the molecular structure predicted by proton NMR and FT-IR spectroscopy.

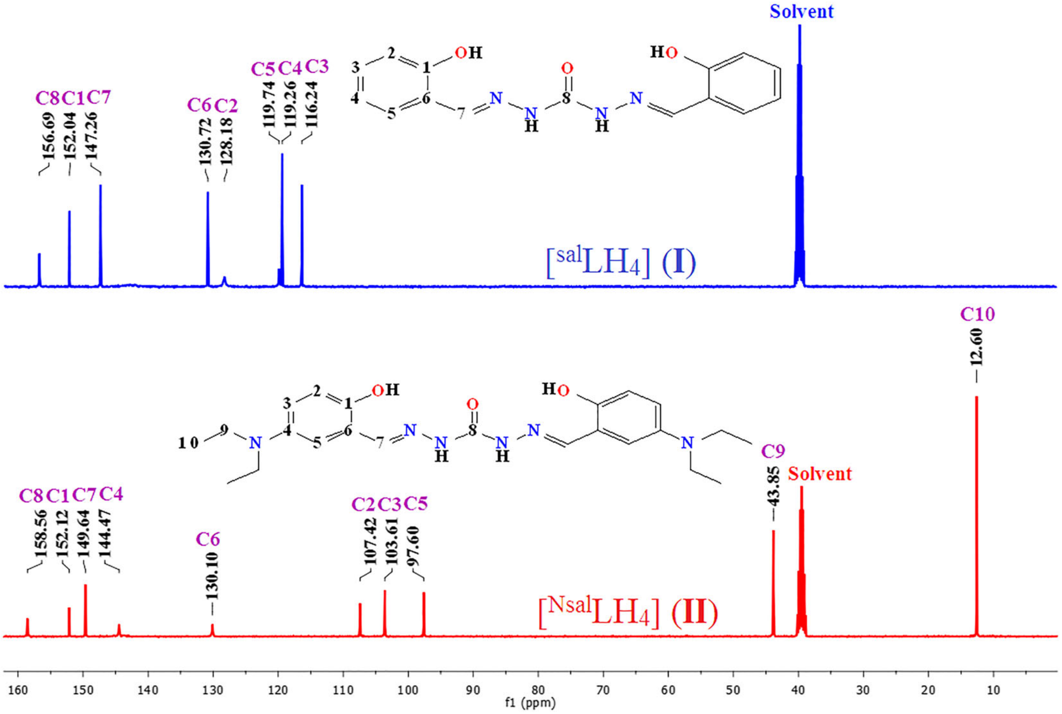

FIGURE 6 ^{13}C NMR spectra of ligands [$^{sal}LH_4$] (**I**) and [$^{Nsal}LH_4$] (**II**) recorded in DMSO-d_6

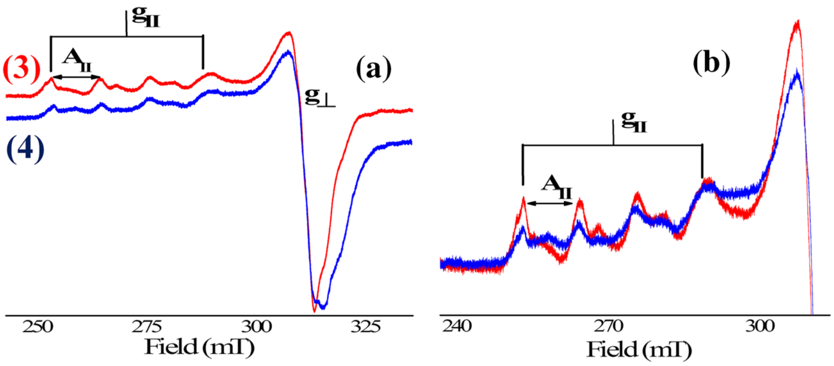

FIGURE 7 (a) X-band EPR spectra of $[(CuCl)_2(^{sal}LH)]$ (**3**) and $[(CuCl)_2(^{Nsal}LH)]$ (**4**) recorded in DMF at liquid nitrogen temperature, (b) the expanded g|| region of the **3** and **4**

X-band EPR spectra of the copper complexes $[H_3O][(CuCl)_2(^{sal}LH)]$ (**3**) and $[H_3O][(CuCl)_2(^{Nsal}LH)]$ (**4**) were recorded at liquid nitrogen temperature in DMF which are presented in Figure 7. It is interesting to note that complexes **3** and **4** generate well-resolved hyperfine splitting pattern in the parallel region with four groups of peaks with an average splitting of 111 and 112 G, respectively. Close observation reveals (Figure 7b) that each group of peaks is comprised of two closely associated peaks.

This is because of the fact that two differently positioned but similar types of copper(II) nuclear spin ($I = 3/2$) interact with the spin of its unpaired electron ($I = 1/2$), and their hyperfine structures mutually overlap with each other. Hence, recorded EPR spectra imply the presence of two magnetically different copper(II) centers in the molecules **3** and **4.** Other groups have reported similar types of magnetically different dicopper(II) centers present in the same molecule where the spin–spin exchange interaction among the copper(II) centers was observed.[21] The axially symmetrically EPR spectra of the complexes **3** and **4** do not produce any forbidden $\Delta\ m_S = \pm 2$ transition at the half field, which rules out the possibility of spin coupling between the two copper(II) centers through the ligand frame.

The calculated principal components of g tensor for **3** are $g_{||} = 2.3998$ and $g\perp = 2.0895$, whereas complex **4** shows $g_{||} = 2.4044$ and $g\perp = 2.0889$ (listed in the Table 2). The EPR spectra of both copper(II) complexes show $g_{||} > g\perp > g_e$, which is the characteristic feature of a distorted square planar metal center.[21b,22]

4.3 | Thermal analysis (TGA/DTA analysis)

The thermal stability of the metal complexes **1–4** was examined by TGA/DTA method under the nitrogen atmosphere at a temperature rate of 10°C/min over a temperature range of 30–915°C and displayed in Figure 8.

Initially, all four metal complexes **1–4** experience a minor mass loss due to the elimination of entrapped solvents, as evident from the single-crystal XRD analysis of **1**. Later on, they follow the multistep breakdown process where partial decomposition of ligands or metal complexes starts. From the TGA/DTA analysis, it is clear that the complexes **1–4** are thermally stable up to 211°C, 241°C, 290°C, and 190°C, respectively. Hence, complexes **1–4** can be easily applied as a catalyst under moderate temperature without breaking their molecular integrity.

4.4 | Catalytic oxidation of alkenes

After a thorough characterization of vanadium and copper complexes **1–4**, their catalytic aptitude was examined and compared for the oxidation of alkenes. Oxidation of alkene produces oxygenated functionalization in the molecule, which is extremely important for the production of fine chemicals. Catalytic oxidation of alkenes was scrutinized using styrene and vanadium-based complex $[H_3O][(VO_2)_2(^{sal}LH)]$ (**1**) as a model substrate and catalysts, respectively. Catalytic oxidation of styrene in the

TABLE 2 Data of spine Hamilton parameter of **3** and **4** in DMF solution at LNT.

	$[H_3O][(CuCl)_2(^{sal}LH)]$ (3)		$[H_3O][(CuCl)_2(^{Nsal}LH)]$ (4)	
Property		$A_{\|\|}$		$A_{\|\|}$
$g_{\|\|}$	2.3998	111 G	2.4044	112 G
$g\perp$	2.0895		2.0889	

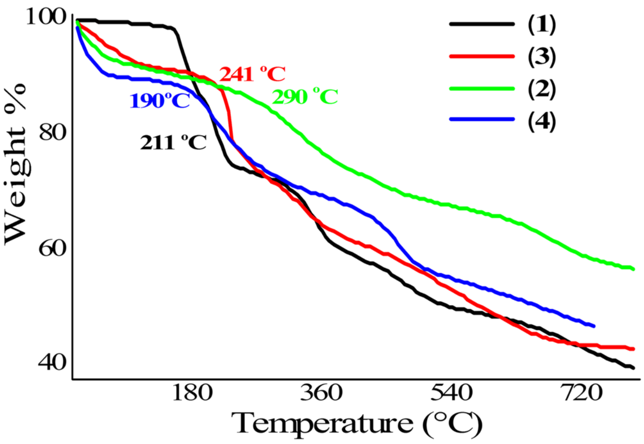

FIGURE 8 TGA plot of $[H_3O][(VO_2)_2(^{sal}LH)]$ (**1**), $[H_3O][(VO_2)_2(^{Nsal}LH)]$ (**2**), $[(CuCl)_2(^{sal}LH)]$ (**3**), and $[(CuCl)_2(^{Nsal}LH)]$ (**4**)

presence of hydrogen peroxide produces mainly benzoic acid and 1-phenylethane-1,2 diol, along with a small amount of acetophenone and benzaldehyde (shown in the Scheme 2), which are commonly reported in the literature.[2c,6,23]

The measurable reaction parameters were precisely optimized to attain the maximum substrate conversion (%) by varying the reaction parameters, namely, catalyst amount, oxidant amount, solvent amount, nature of solvents, types of oxidants, and temperature. Moreover, the impact of the metal center on the catalytic oxidation of alkenes was checked by using the copper counterpart of catalyst **1** under similar optimized conditions.

Four different quantities, i.e., 0.041, 0.125, 0.208, and 0.291 mol% of catalyst were screened to optimize the effect of catalyst (**1**) amounts on the oxidation of styrene while using a fixed amount of styrene (0.520 g, 5 mmol) and 30% H_2O_2 (1.700 g, 15 mmol) in 5 ml of methanol at 60°C for 6 h. The outcomes are shown in Figure 9a. While increasing the quantity of catalyst from 0.041 g to 0.125 mol%, a massive improvement in substrate conversion(%) (from 29% to 86%) was observed. However, a further rise in the catalyst amount does not increase the substrate conversion(%) much. Hence, 0.125 mol% of catalyst was considered as optimum.

The influence of oxidant amount on oxidation reaction was studied by using four different substrates to oxidant molar ratios, namely, 1:1, 1:2, 1:3, and 1:4. Only 51% of substrate conversion was achieved by using 1:1 substrates to oxidant molar ratio (Figure 9b), whereas 1:2 and 1:3 produce comparable substrate conversion(%). Slight decline in the substrate conversion can be seen while using 1:4 substrates to oxidant molar ratio. In order to optimize the volume of solvent during the catalytic oxidation of styrene, four different volumes of methanol, that is, 2.5, 5, 7.5, and 10 ml were tested while keeping all the other parameters fixed. The corresponding effects are shown in Figure 9c. With a rise in the volume of solvent from 2.5 to 10 ml, substrate conversion(%) decreases gradually due to the reduction of the effective collision among the reactant molecules in a larger volume of solvent. A small reduction (2%) in the substrate conversion (%) is observed while increasing the solvent amount from 2.5 to 5 ml. However, 5 ml volume was chosen as optimum to avoid the inherent errors associated with the handling of the smaller volume of the solvent.

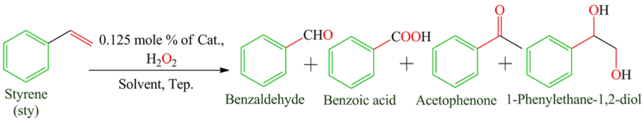

SCHEME 2 Oxidation products of styrene catalyzed by **1**–**4** in the presence of hydrogen peroxide at 70°C bath temperature

The nature of the solvent has a strong influence on the catalytic oxidation of styrene in the presence of hydrogen peroxide. Three different types of solvents, DMF, CH_3CN, and MeOH, were used as a reaction medium while keeping other parameters the same. The impact of the nature of solvents is displayed in Figure 9d. A maximum substrate conversion(%) of 85% was achieved in methanol. Nevertheless, with decreasing the polarity of the solvent, substrate conversion decreases, and hence, in acetonitrile, 42% of conversion was achieved. However, only 2% conversion was observed in DMF, which may be due to the higher distribution ratio of the oxidation products in DMF.

Similarly, to choose the suitable oxidizing agents, oxidation of styrene was executed with two different oxidants, such as 30% H_2O_2 and TBHP, and the result is shown in Figure 9e. TBHP shows only 36% conversion, whereas up to 85% conversion can be achieved with hydrogen peroxide. Mainly two factors are responsible for the lower activity of TBHP. One, during the catalytic reaction, metal complexes **1**–**4** reacts with the available peroxide to form metal peroxides, which are responsible for the alkene oxidation, and the metal peroxides which are generated in the presence of TBHP are relatively weaker in nature in comparison to the hydrogen peroxide drove metal peroxides. Two steric bulkiness can cause trouble for an easy substrate association with the metal center in case of TBHP containing metal peroxides.

Finally, the influence of bath temperature was studied by monitoring the styrene oxidation in five different bath temperatures, 50°C, 55°C, 60°C, 65°C, and 70°C (shown in Figure 9f). With the rising bath temperature, substrate conversion(%) increases gradually, and a maximum of 94% conversion was achieved at 70°C. Hence, 70°C of bath temperature was considered as

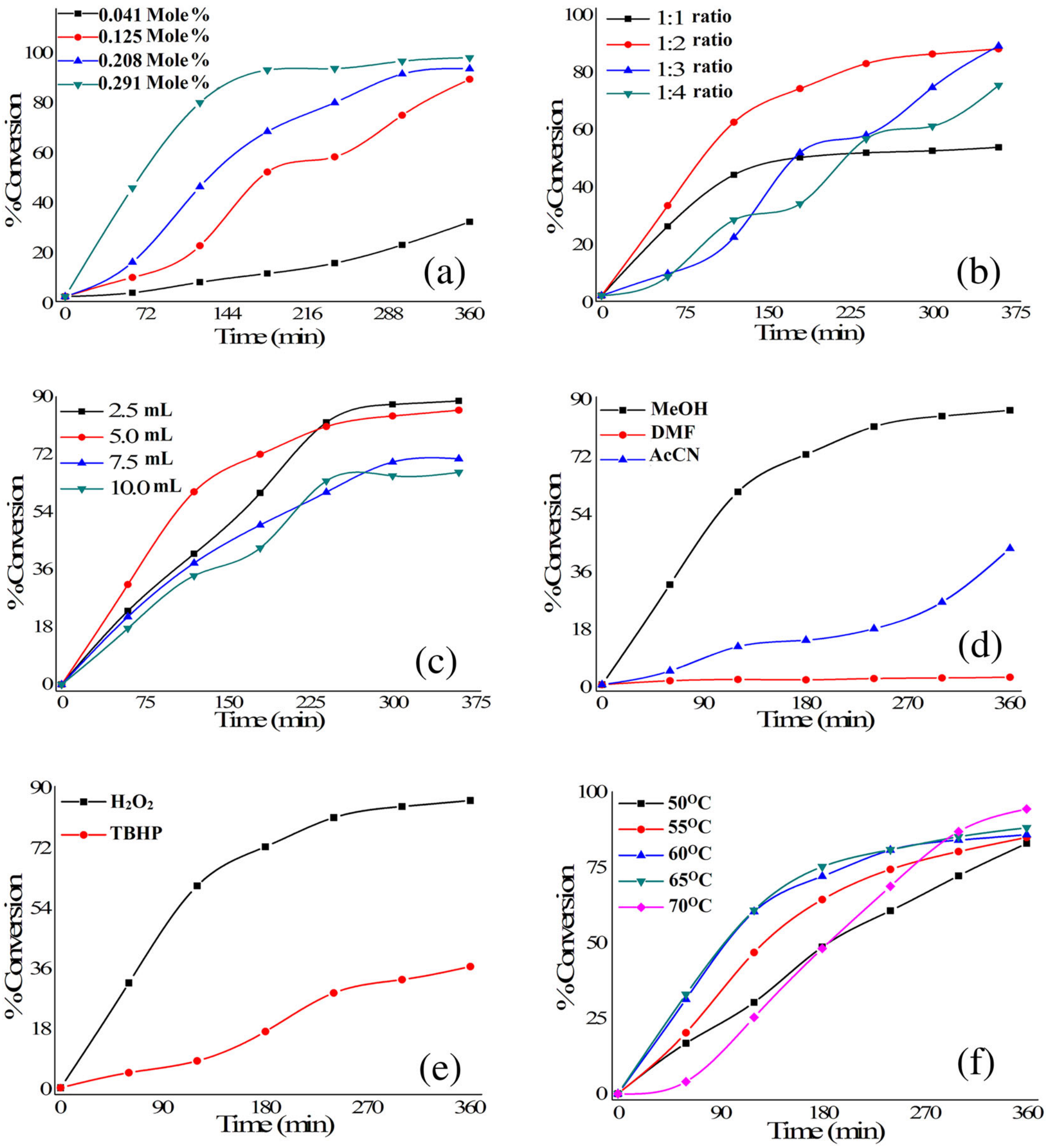

FIGURE 9 Optimization of catalytic oxidation of styrene with the catalyst $[H_3O][(VO_2)_2(^{sal}LH)]$ (**1**): (a) effect of catalyst amount, (b) effect of 30% H_2O_2 amount, (c) impact of solvent amount, (d) influence of nature of the solvent, (e) influence of nature of oxidant, and (f) effect of temperature

optimum. The final optimized reaction conditions are 0.125 mol% of catalyst **1**, H_2O_2 as an oxidant, MeOH as a solvent, oxidant:substrate ratio of 1:2, 5 ml of solvent, 70°C bath temperature, and 6 h of reaction time (listed in entry no. 17 of Table 3).

Under the above-optimized reaction conditions, catalyst **2** shows comparable substrate conversion (93%) to that of the catalyst **1** (94%). However, in terms of efficiency, catalyst **2** shows a little higher turnover frequency (TOF) (= 80.61 h^{-1}) values compared with cat **1** (TOF = 62.76 h^{-1}). To observe the impact of metal centers in the catalytic reaction, corresponding copper catalysts **3** and **4** were also applied for the styrene oxidation under the same optimized reaction conditions. It is evident from the data that copper catalysts **3** and **4** are not as efficient as their vanadium counterparts in terms of substrate conversion(%) or efficiency. Catalyst **3** displays 41% conversion with TOF values of 28.50 h^{-1}, whereas 37% conversion with TOF value of 33.81 h^{-1} is shown by catalyst **4.** With more than 50% product selectivity, benzoic acid (in methanolic solution it converts into methyl benzoate) appears as a major product in every case.

The blank reaction of styrene oxidation without catalyst shows only 5% conversion. Moreover, in the presence of the metal precursors, $VO(acac)_2$ and $CuCl_2$, oxidation of styrene was monitored and displayed in Figures 10 and 11. Data confirm that styrene oxidation under

TABLE 3 Data for all the parameters applied to optimize for maximum conversion of styrene oxidation by catalyst $[H_3O][(VO_2)_2(^{sal}LH)]$ (**1**).

S.N.	Mole % of Cat.	Temp. (°C)	Sub.:Oxi.	Oxidant	Solvent (ml)	Solvent	% Conv.	TOF (h^{-1})
1	0.0416	60	1:3	H_2O_2	5	MeOH	29	59.62
2	0.125	60	1:3	H_2O_2	5	MeOH	86	57.88
3	0.208	60	1:3	H_2O_2	5	MeOH	91	36.41
4	0.291	60	1:3	H_2O_2	5	MeOH	95	27.26
5	0.125	60	1:1	H_2O_2	5	MeOH	51	34.41
6	0.125	60	1:2	H_2O_2	5	MeOH	85	57.22
7	0.125	60	1:4	H_2O_2	5	MeOH	73	48.75
8	0.125	60	1:2	H_2O_2	2.5	MeOH	88	59.15
9	0.125	60	1:2	H_2O_2	7.5	MeOH	70	47.08
10	0.125	60	1:2	H_2O_2	10	MeOH	66	44.28
11	0.125	60	1:2	H_2O_2	5	DMF	2	1.40
12	0.125	60	1:2	H_2O_2	5	AcCN	42	28.41
13	0.125	60	1:2	TBHP	5	MeOH	36	24.14
14	0.125	50	1:2	H_2O_2	5	MeOH	82	55.28
15	0.125	55	1:2	H_2O_2	5	MeOH	84	56.62
16	0.125	65	1:2	H_2O_2	5	MeOH	88	58.75
17	0.125	70	1:2	H_2O_2	5	MeOH	94	62.89

Abbreviation: TOF, turnover frequency.

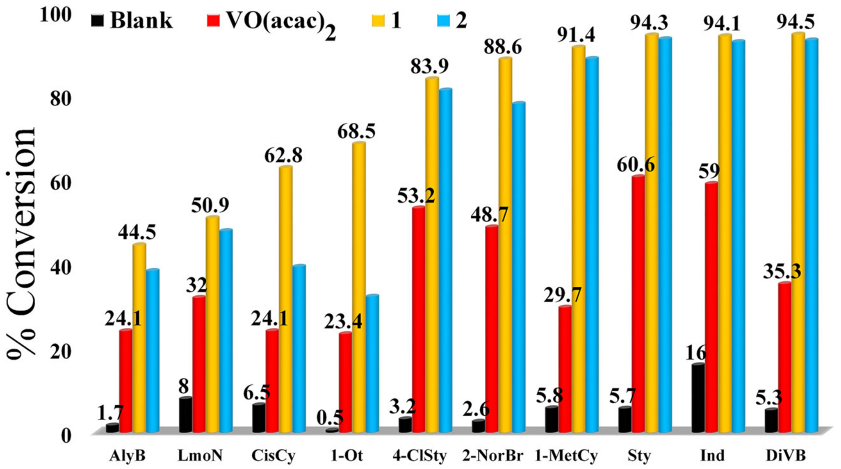

FIGURE 10 Comparison of % conversion of blank reaction with the catalysts and their respective metal salts under optimized reaction conditions

optimized reaction conditions in the presence of metal precursors $VO(acac)_2$ and $CuCl_2$ proceeds with 60% and 28% substrate conversion, respectively. So, this implies that the vanadium and copper centers are catalytically active and essential for the styrene oxidation. However, while using catalysts **1–4**, a substantial improvement of substrate conversion(%) is visible in comparison to the metal precursors. It justifies that not only metal centers, but the associated ligand frame is equally important and necessary for the efficient function of the catalyst. Hence, the current ligand system is boosting the styrene oxidation efficiency of the vanadium as well as the copper centers. The data suggest that in comparison to the vanadium-based catalysts **1–2**, copper-based catalysts are quite less effective (except 1-octene) towards styrene oxidation in terms of substrate conversion and efficiency (Table 4). The plausible reason for the lower efficiency of copper catalysts **3–4** in comparison with their vanadium counterparts is because vanadium makes stronger metal peroxides than copper, which are the active species responsible for the catalytic oxidation.

We extended our study to the oxidation of a number of aromatic and aliphatic alkenes, and the results are summarized in Table 4. Each alkene was oxidized in the

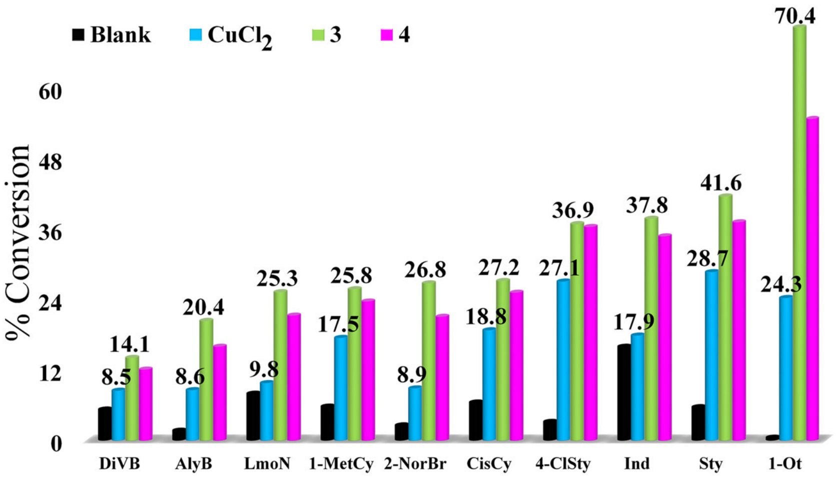

FIGURE 11 Comparison of % conversion of blank reaction with the catalysts and their respective metal salts under optimized reaction conditions

presence of catalysts **1–4**, and the obtained conversion(%) was compared with the metal precursor catalyzed reactions as well as the blank reactions. Comparison of substrate conversion(%) achieved in the presence of the catalysts **1–4** and their metal precursors along with the blank reactions is plotted and displayed in Figures 10 and 11.

Some interesting aspects of alkene oxidation can be observed while analyzing the data acquired in the presence of catalysts **1–4**. Broadly, two classes of compounds, that is, aromatic and aliphatic alkenes, were used for the experimental purpose. Out of the listed 10 olefins, five are aromatic, and five are aliphatic. Under the optimized reaction conditions, in general, aromatic olefins show higher substrate conversion(%) in the presence of vanadium-based catalysts **1** and **2**. Styrene, divinylbenzene, and indene are showing comparable substrate conversion (>94%). 4-Chlorostyrene shows 83% conversion, whereas the least conversion(%) is observed in allyl benzene (44%). In olefins like styrene, divinylbenzene, and indene, the ethylenic double bond is electron rich because of its conjugation with the phenyl ring. Therefore, these olefins can easily participate in the oxidation process. Although in 4-chlorostyrene, the presence of electron-withdrawing group (—Cl) at the *p*-position of the phenyl group depletes the electron density from the ethylenic double bond, thereby making them less active towards oxidation purpose. On the other hand, in allyl benzene, there is no conjugation between the π-electrons of the phenyl ring and the π-electrons of the ethylenic double bond. Hence, it acts like an aliphatic alkene and makes it least active among all the listed aromatic alkenes. Thus, electron-rich alkenes undergo oxidation reaction easily in the presence of vanadium-based catalysts **1** and **2**. By similarly considering the electronic effect, among all the studied aliphatic alkenes, 1-methylcyclohex-1-ene shows the highest substrate conversion (91%) in the presence of catalyst **1**. The order of substrate conversion for other aliphatic alkenes in the presence of catalyst **1** is 2-norbornene (88%) > 1-octene (68%) > *cis*-cyclooctene (62%) > limonene (50%). Catalyst **2** delivers the same order of reactivity with the listed aromatic alkenes, but aliphatic alkenes show a different order of reactivity than the catalyst **1,** which is, 1-methylcyclohex-1-ene (88%) > 2-norbornene (78%) > limonene (47%) > *cis*-cyclooctene (39%) > 1-octene (32%). It seems that electronic factors no longer controlled the reactivity pattern in aliphatic alkenes, especially among limonene, *cis*-cyclooctene, and 1-octene. A second factor, probably the steric effect cooperation with electronic factor decides the reactivity pattern of these alkenes in the presence of catalysts **1** and **2**.

While analyzing the data of oxidation of alkenes using copper-based catalysts **3** and **4**, it appears that the second factor, that is, steric bulkiness, contributes more than the electronic factor in deciding the reactivity of listed alkenes towards oxidation. Hence, the listed alkenes come out more random in the reactivity pattern. Styrene and *cis*-cyclooctene show higher substrate conversion(%) among the aromatic and aliphatic alkenes, respectively. Irrespective of alkenes, [$^{\mathrm{Nsal}}\mathrm{LH}_4$] (**II**)-based vanadium and copper catalysts perform less effectively in comparison with the [$^{\mathrm{sal}}\mathrm{LH}_4$] (**I**)-based vanadium and copper catalysts. The presence of electron-donating group *N*,*N*-diethylamine at the *p*-position in the ligand (**II**) leads to the formation of weaker metal peroxo complexes compared to the ligand (**I**)-based metal peroxo complexes, and it is evident from the catalytic data that the latter metal peroxo complexes (ligand (**I**)-based complexes) outperform the former ones (ligand (**II**)-based complexes). Detailed product selectivity of the oxidation of various alkenes is summarized in Table 5.

It should be noted that in the methanolic solution, no carboxylic acid was detected due to the conversion of carboxylic acids into the corresponding methyl esters. In

TABLE 4 Conversion(%) and TOF values of oxidation of various alkenes using all the catalysts (**1–4)** in the presence of H_2O_2 in 5 ml MeOH at 70°C temperature.

S.N.	Cat.	Substrate	% conversion	TOF (h^{-1})	Reference
1	**1**	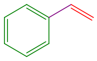	94	62.89	[29]
	2		93	80.74	
	3		41	29.59	
	4		37	33.81	
2	**1**	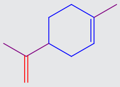	50	33.94	[30,31]
	2		47	41.32	
	3		25	18.00	
	4		21	19.36	
3	**1**	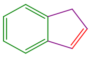	94	62.75	[29d,32]
	2		92	80.13	
	3		37	26.89	
	4		34	31.63	
4	**1**	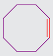	62	41.88	[33,34]
	2		39	34.06	
	3		27	19.35	
	4		25	22.90	
5	**1**	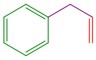	44	29.67	[35]
	2		38	33.19	
	3		20	14.51	
	4		16	14.54	
6	**1**	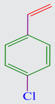	83	55.95	[2b]
	2		81	70.19	
	3		36	26.25	
	4		36	33.09	
7	**1**	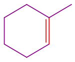	91	60.95	[27,36]
	2		88	76.67	
	3		25	18.35	
	4		23	21.54	
8	**1**		68	45.68	[2b,29d,32,37]
	2		32	27.92	
	3		70	50.09	
	4		54	49.81	
9	**1**	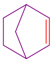	88	59.08	[27,32]
	2		78	67.42	
	3		26	19.06	
	4		21	19.18	

(Continues)

TABLE 4 (Continued)

S.N.	Cat.	Substrate	% conversion	TOF (h^{-1})	Reference
10	**1**	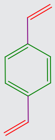	94	63.02	
	2		93	80.48	
	3		14	10.03	
	4		12	10.99	

Abbreviation: TOF, turnover frequency.

TABLE 5 Result of oxidation of olefins catalyzed by **1**–**4**

S.N.	Cat.	% con.	TOF (h^{-1})	% selectivity of products			
1		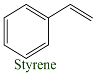 Styrene (sty)		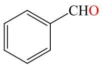 Benzaldehyde	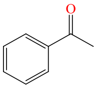 Acetophenone	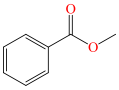 Methyl benzoate	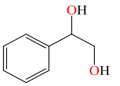 1-Phenylethane-1,2-diol
	1	94	62.89	10.6	7.8	59.5	21.9
	2	93	80.74	12.4	11.2	55.9	20.2
	3	41	29.59	22.9	22.4	50.1	4.4
	4	37	33.81	30.5	17.4	46.9	5.0
2		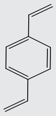 Divinylbenzene (DiVB)		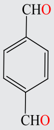 Terephthalaldehyde	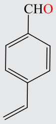 4-vinylbenzaldehyde	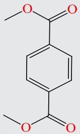 Dimethyl terephthalate	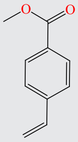 Methyl 4-vinylbenzoate
	1	94	63.02	15.7	7.7	23.9	52.5
	2	93	80.48	16.1	7.2	17.3	59.1
	3	14	10.03	22.8	40.0	17.6	19.3
	4	12	10.99	21.3	38.5	18.9	21.1
3		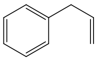 Allylbenzene (AlyB)		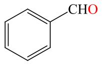 Benzaldehyde	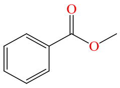 Methyl benzoate	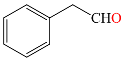 Phenylacetaldehyde	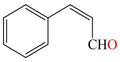 Phenylacrylaldehyde
	1	44	29.67	26.9	52.4	6.6	13.9
	2	38	33.19	23.7	55.1	7.4	13.5
	3	20	14.51	26.2	37.4	12.0	24.2
	4	16	14.54	32.9	36.4	8.8	21.6

TABLE 5 (Continued)

S.N.	Cat.	% con.	TOF (h^{-1})	% selectivity of products			
4							
			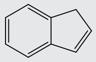 Indene (Ind)	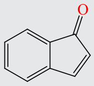 Indenone	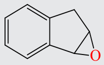 Dihydro-indeno oxirene	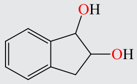 Dihydro-indene- 1,2-diol	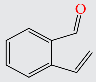 2-Vinyl benzaldehyde
	1	94	62.75	62.6	5.5	63.7	18.5
	2	92	80.13	80.0	3.6	58.3	23.2
	3	37	26.89	25.8	13.5	31.9	32.7
	4	34	31.63	30.6	21.1	28.4	28.8
5							
			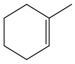 1-Methylcyclo hex-1-ene (1-MetCy)	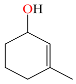 3-Methyl cyclohex-2-enol	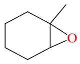 1-Methyl-7- oxabicycloheptane	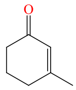 3-Methylcyclohex- 2-enone	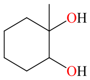 1-Methylcyclo hexane-1,2-diol
	1	91	60.95	8.5	20.6	17.9	52.8
	2	88	76.67	9.3	23.5	12.9	54.0
	3	25	18.35	9.5	33.4	33.2	23.8
	4	23	21.54	9.1	28.4	27.8	34.4
6							
			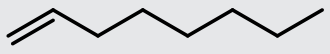 1-Octene (1-Ot)	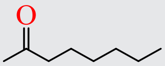 Octan-2-one	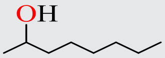 Octan-2-ol	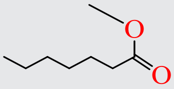 Methyl heptanoate	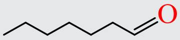 Heptanal
	1	68	45.68	38.5	32.0	29.4	—
	2	32	27.92	39.0	35.0	25.8	—
	3	70	50.09	43.4	27.2	15.7	13.6
	4	54	49.81	50.9	26.0	12.4	10.5
7							—
			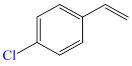 4-Chlorostyrene 4-ClSty	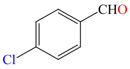 4-Chloro benzaldehyde	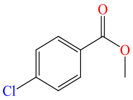 Methyl 4-chloro benzoate	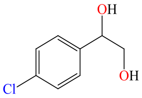 1-(4-Chlorophenyl) ethane-1,2-diol	
	1	83	55.95	9.3	51.8	38.8	—
	2	81	70.19	11.4	61.4	27.1	—
	3	36	26.25	19.2	71.3	9.4	—
	4	36	33.09	20.0	68.6	11.3	—
8							—
			 2-Norbornene (2-NorBr)	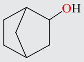 2-Bicycloheptanol	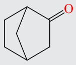 2-Bicycloheptanone	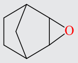 3-Oxatricyclooctane	

(Continues)

TABLE 5 (Continued)

S.N.	Cat.	% con.	TOF (h^{-1})	% selectivity of products			
	1	88	59.08	12.5	4.1	83.3	—
	2	78	67.42	9.4	3.1	86.9	—
	3	26	19.06	9.5	38.2	52.2	—
	4	21	19.18	10.7	34.1	55.1	—
9							—
			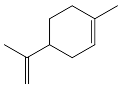 1-Methyl-4-(prop-1-en-2-yl)cyclohex-1-ene(Limonene) (LmoN)	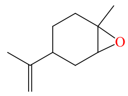 1-Methyl-4-(prop-1-en-2-yl)-7-oxabicycloheptane	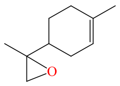 2-Methyl-2-(4-methylcyclohex-3-en-1-yl)oxirane	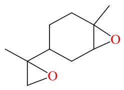 1-Methyl-4-(2-methyloxiran-2-yl)-7-oxabicycloheptane	
	1	50	33.94	33.8	23.1	51.7	—
	2	47	41.32	41.2	25.0	48.0	—
	3	25	18.00	17.3	17.4	33.9	—
	4	21	19.36	18.7	14.4	37.8	—
10						—	—
			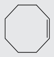 Cis-cyclooctene (CisCy)	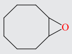 Oxabicyclononane	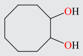 Cyclooctane-1,2-diol		
	1	62	41.88	92.3	7.6	—	—
	2	39	34.06	97.3	2.6	—	—
	3	27	19.35	65.0	34.9	—	—
	4	25	22.90	67.3	32.6	—	—

Note. Products selectivity(%), substrate conversion(%), and TOF value observed under optimized reaction conditions.
Abbreviation: TOF, turnover frequency.

other solvents, such as acetonitrile, the carboxylic acid can be detected.

Even though the reaction mechanism of the catalytic oxidation of alkenes was not studied in the present work, a number of reports can be found in the literature[2c,24–26] discussing the detailed mechanism of similar systems. Based on our electronic spectroscopic studies and earlier reports, it is anticipated that in the first step, the metal complex converts into the peroxo species by reacting with hydrogen peroxide. This active metal peroxo species goes back to its native form by oxidizing the available alkenes. We did not detect the active metal peroxo complexes directly. The gradual addition of 1 drop portion of 0.1 M H_2O_2 into the methanolic solution of $[H_3O][(VO_2)_2(^{sal}LH)]$ (**1**) complex (6.99×10^{-4} M) causes the disappearance of the 390-nm band, while a new band generates at 320 nm, and the 280 nm band intensifies without changing its λ_{max} (shown in Figure 12). All these

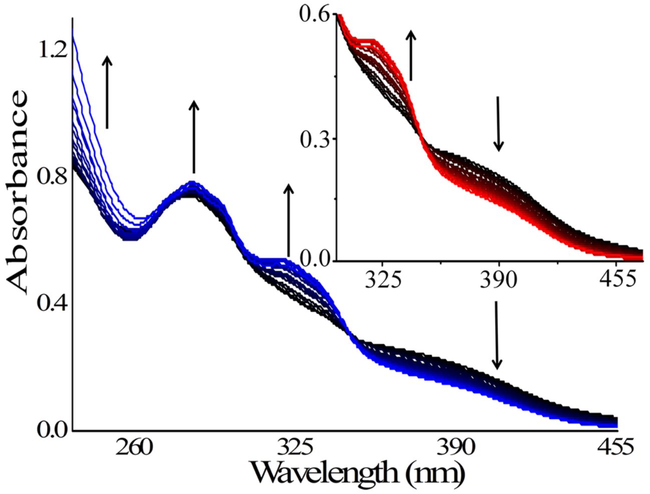

FIGURE 12 Spectral changes observed during the progressive addition one drop of 0.1M H_2O_2 in the 6.99×10^{-4} M methanolic solution of $[H_3O][(VO_2)_2(^{sal}LH)]$ (**1**) complex

changes indicate the formation of $[(VO_2)_2(^{sal}LH)]$-peroxido species in solution.[6a,27,28] In the presence of properly diluted H_2O_2, complexes **2–4** also exhibit the electronic spectral changes characteristic of metal peroxo species in solution (shown in Figures S10–S12). The *d-d* transitions of complexes **3** and **4** disappear by incremental addition of 0.1 M 30% H_2O_2 solution into a 3.67×10^{-4} M methanolic solution of **3** and 5.60×10^{-4} M methanolic solution of **4**, which further supports the formation of Cu^{3+}-peroxo species in the solution.[2c,22c,29c] Spectral changes have been shown in Figures 3 and S8.

5 | CONCLUSION

Two unique and rare bimetallic vanadium complexes $[H_3O][(VO_2)_2(^{sal}LH)]$ (**1**) and $[H_3O][(VO_2)_2(^{Nsal}LH)]$ (**2**) were successfully synthesized. Molecular structures and properties of the complexes **1** and **2** were thoroughly analyzed via a number of spectroscopic and thermal studies. Single-crystal X-ray analysis was used to confirm the proposed molecular structure of complex **1** in solid-state**.** Both the vanadium centers are in the +5 oxidation state in complexes **1** and **2.** Bimetallic vanadium complexes **1** and **2** act as an effective catalyst for the oxidation of several aromatic and aliphatic alkenes. It was observed that electron-rich alkenes are easy to oxidize; hence, in general, aromatic alkenes with electron donor groups are performing better than the electron-deficient aliphatic alkenes. To investigate the effect of the metal center in the alkene oxidation, copper complexes $[H_3O][(CuCl)_2(^{sal}LH)]$ (**3**) and $[H_3O][(CuCl)_2(^{Nsal}LH)]$ (**4**) were synthesized using the same ligand systems **I** and **II** which were used for the preparation of vanadium complexes and characterized in detail. Surprisingly, copper-based catalysts **3** and **4** act less efficiently towards the oxidation of the alkenes under the same optimized reaction conditions set for the vanadium complexes. Furthermore, the ligand $[^{Nsal}LH_4]$ (**II**) with an electron-donating group makes relatively weaker oxidation catalysts as compared with $[^{sal}LH_4]$ (**I**). Therefore, irrespective of alkenes, bimetallic complexes **1** and **3** overperform **2** and **4**. Although the performance of copper-based catalysts is not very impressive for the listed alkenes, their vanadium counterparts are extremely effective and efficient in comparison with the currently available vanadium-based homogeneous catalysts.

ACKNOWLEDGEMENTS

C. H. thanks the Science and Engineering Research Board (SERB), DST, the Government of India, New Delhi, for financial support (grant no. SB/EMEQ-055/2014) of the work. A. M. is thankful to IIT (ISM) Dhanbad for fellowship. The authors would like to thank SAIF Mumbai for TGA/DTA and X-band EPR analysis. The authors acknowledge CFR IIT (ISM) Dhanbad for providing single-crystal XRD analysis. The authors also acknowledge SAIF Punjab University for ESI-MS data. The authors would like to thank DST-FIST (project no. SR/FST/CSI-256) for 400 MHz NMR facility in the department of chemistry IIT (ISM) Dhanbad. GC used in this study was procured from the grant given by Science and Engineering Research Board (SERB), Department of Science and Technology (DST) (grant no SB/FT/CS-027/2014), Government of India, New Delhi, India, to C. H. The authors would like to thanks Dr. Nikita Chaudhary for helping in writing the manuscript. Special thanks to Dr. H. P. Nayek, Department of Chemistry for the X-ray crystallographic studies.

AUTHOR CONTRIBUTIONS

Abhishek Maurya: Conceptualization; investigation. **Chanchal Haldar:** Data curation; formal analysis; funding acquisition; methodology; project administration; resources; software; supervision; validation; visualization.

CONFLICT OF INTEREST

There are no conflicts of interest to declare.

SUPPLEMENTARY INFORMATION

Additional data on single-crystal XRD, FI-IR, UV–Vis, ^1H, and ^{13}C NMR, and catalytic activity can be found in the supporting information.

DATA AVAILABILITY STATEMENT

The data that support the findings of this study are available in the supplementary material of this article.

ORCID

Abhishek Maurya https://orcid.org/0000-0001-6977-9532
Chanchal Haldar https://orcid.org/0000-0003-4642-7918

REFERENCES

[1] a) S. G. V. Ornum, R. M. Champeau, R. Pariza, *Chem. Rev.* **2006**, *106*, 2990; b) S. S. Acharyya, S. Ghosh, R. Tiwari, B. Sarkar, R. K. Singha, C. Pendem, T. Sasaki, R. Bal, *Green Chem.* **2014**, *16*, 2500; c) U. Biermann, U. Bornscheuer, M. A. R. Meier, J. O. Metzger, H. J. Schäfer, *Angew. Chem., Int. Ed.* **2011**, *50*, 3854; d) F. A. R. Ruiz, J. A. O. Ruiz, *Energy Fuels* **2016**, 30.

[2] a) R. R. Langeslay, D. M. Kaphan, C. L. Marshall, P. C. Stair, A. P. Sattelberger, M. Delferro, *Chem. Rev.* **2019**, *119*, 2128;

b) P. Paul, A. Ghosh, S. Chatterjee, A. Bera, S. M. Alam, S. M. Islam, *Inorg. Chim. Acta* **2019**, *492*, 198; c) A. Maurya, N. Kesharwani, P. Kachhap, V. K. Mishra, N. Chaudhary, C. Haldar, *Appl. Organomet. Chem.* **2019**, 33.

[3] H. Wang, J. Yamamoto, *Am. Chem. Soc.* **2014**, *136*, 1222.

[4] a) A. Rezaeifard, R. Haddad, M. Jafarpour, M. Hakimi, *J. Am. Chem. Soc.* **2013**, *135*, 10036; b) T. Bunchuay, R. Ketkaew, P. Chotmongkolsap, T. Chutimasakul, J. Kanarat, Y. Tantirungrotechai, J. Tantirungrotechai, *Catal. Sci. Technol.* **2017**, *7*, 6069; c) Z. P. Pai, N. V. Selivanova, P. V. Oleneva, P. V. Berdnikova, A. M. Beskopyl'nyi, *Catal. Commun.* **2017**, *88*, 45.

[5] a) M. R. Maurya, C. Haldar, A. A. Khan, A. Azam, A. Salahuddin, A. Kumar, J. C. Pessoa, *Eur. J. Inorg. Chem.* **2012**, *15*, 2560; b) J. Piera, J. E. Bäckvall, *Angew. Chem., Int. Ed.* **2008**, *47*, 3506; c) M. Amini, M. M. Haghdoost, M. Bagherzadeh, *Coord. Chem. Rev.* **2014**, *268*, 83; d) J. A. L. da Silva, J. J. R. F. da Silva, A. J. L. Pombeiro, *Coord. Chem. Rev.* **2011**, *255*, 2232.

[6] a) M. Sutradhar, L. M. D. R. S. Martins, M. F. C. G. da Silva, A. J. L. Pombeiro, *Coord. Chem. Rev.* **2015**, *301*, 200; b) M. R. Maurya, *Coord. Chem. Rev.* **2019**, *383*, 43.

[7] a) W. Jiang, J. D. Gorden, C. R. Goldsmith, *Inorg. Chem.* **2012**, *51*, 2725; b) V. K. Singh, A. Maurya, N. Kesharwani, P. Kachhap, S. Kumari, A. K. Mahato, V. K. Mishra, C. Haldar, *J. Coord. Chem.* **2018**, *71*, 520; c) M. Sankaralingam, M. Balamurugan, M. Palaniandavar, *Coord. Chem. Rev.* **2020**, *403*, 213085.

[8] a) N. P. Jayaweera, A. E. Hall, A. A. Wilson, M. E. Konkle, K. A. Wheeler, R. F. Semeniuc, *Inorganica Chim. Acta* **2020**, *506*, 119507; b) A. Bocian, A. Gorczyński, D. Marcinkowski, S. Witomska, M. Kubicki, P. Mech, M. Bogunia, J. Brzeski, M. Makowski, P. Pawluć, V. Patroniak, *J. Mol. Liq.* **2020**, *302*, 112590; c) P. Gamez, P. G. Aubel, W. L. Driessen, J. Reedijk, *Chem. Soc. Rev.* **2001**, *30*, 376; d) L. S. Shulpina, M. M. Vinogradov, Y. N. Kozlov, Y. V. Nelyubina, N. S. Ikonnikov, G. B. Shulpin, *Inorganica Chim. Acta* **2020**, *512*, 119889; e) T. Punniyamurthy, L. Rout, *Coord. Chem. Rev.* **2008**, *252*, 134; f) M. Sutradhar, L. M. Martins, T. Roy Barman, M. L. Kuznetsov, M. F. C. G. da Silva, A. J. L. Pombeiro, *New J. Chem.* **2019**, *43*, 17557; g) J. Shi, Y. Wei, Y. Zhang, J. Tang, H. Bian, Q. Yu, F. Huang, *Polyhedron* **2019**, *162*, 81; h) S. D. Kurbaha, N. S. Clovis, *Inorganica Chim. Acta* **2020**, *511*, 119837.

[9] a) H. Pellissier, *Coord. Chem. Rev.* **2015**, *284*, 93; b) N. Yan, C. Xiao, Y. Kou, *Coord. Chem. Rev.* **2010**, *254*, 1179; c) I. K. Biernacka, K. Biernacki, A. L. Magalhães, A. M. Fonseca, I. C. Neves, *J. Catal.* **2011**, *278*, 102.

[10] a) Y. Liu, D. Xue, C. Li, J. Xiao, C. Wang, *Catal. Sci. Technol.* **2017**, *7*, 5510; b) H. Ünver, I. Kani, *J. Chem. Sci.* **2018**, *130*, 33; c) M. Kirihara, *Coord. Chem. Rev.* **2011**, *255*, 2281; d) A. Chieregato, J. M. L. Nieto, F. Cavani, *Coord. Chem. Rev.* **2015**, *301*, 3; e) J. C. Védrine, G. J. Hutchings, C. J. Kiely, *Catal. Today* **2013**, *217*, 57; f) W. Chu, J. Luo, S. Paul, Y. Liu, A. Khodakov, E. Bordes, *Catal. Today* **2017**, *298*, 145.

[11] a) M. Rajasekar, S. Sreedaran, R. Prabu, V. Narayanan, R. Jegadeesh, N. Raaman, A. K. Rahiman, *J. Coord. Chem.* **2010**, *63*, 136; b) M. S. Karthikeyan, D. J. Prasad, B. Poojary, K. S. Bhat, B. S. Holla, N. S. Kumari, *Bioorg. Med. Chem.* **2006**, (14), 7482; c) P. Panneerselvam, R. R. Nair, G. Vijayalakshmi, E. H. Subramanian, S. K. Sridhar, *Eur. J. Med. Chem.* **2005**, *40*, 225; d) N. C. Gianneschi, S. T. Nguyen, C. A. Mirkin, *J. Am. Chem. Soc.* **2005**, *127*, 1644; e) S. Di Bella, I. Fragalà, *New J. Chem.* **2002**, *26*, 285.

[12] a) M. Sutradhar, A. J. Pombeiro, *Coord. Chem. Rev.* **2014**, *265*, 89; b) H. M. A. Hassan, M. A. Betiha, E. A. El-Sharkawy, R. F. M. Elshaarawy, N. B. El-Assy, A. A. Essawy, A. M. Tolba, A. M. Rabie, *Colloid Surf. A Physicochem. Eng. Asp.* **2020**, *591*, 124520.

[13] D. Dragancea, N. Talmaci, S. Shova, G. Novitchi, D. Darvasiova, P. Rapta, M. Breza, M. Galanski, J. Kozısek, N. M. R. Martins, L. M. D. R. S. Martins, A. J. L. Pombeiro, V. B. Arion, *Inorg. Chem.* **2016**, *55*(18), 9187.

[14] R. A. Rowe, M. M. Jones, *Inorg. Synth.* **1957**, *5*, 113.

[15] C. M. Burla, R. Caliandro, M. Camalli, B. Carrozzini, G. L. Cascarano, L. De Caro, C. Giacovazzo, G. Polidori, R. Spagna, *J. Appl. Crystallogr.* **2005**, *38*(2), 381.

[16] G. Sheldrick, *Acta Crystallogr. C.* **2015**, *71*(1), 3.

[17] H. H. Monfared, R. Bikas, P. M. Anarjan, S. W. Ng, E. R. T. Tiekink, *Z. Anorg. Allg. Chem.* **2014**, *640*(1), 243.

[18] a) M. A. Altahan, M. A. Beckett, S. J. Coles, P. N. Horton, *J. Cluster Sci.* **2018**, *29*, 1337; b) L. Zhu, K. Seff, D. H. Olson, B. J. Cohen, R. B. V. Dreele, *J. Phys. Chem. B* **1999**, *103*, 10365; c) A. W. Addison, T. N. Rao, J. Reedijk, J. van Rijn, G. C. Verschoor, *Dalton Trans.* **1984**, 1349.

[19] a) M. R. Maurya, C. Haldar, A. Kumar, M. L. Kuznetsov, F. Avecilla, J. C. Pessoa, *Dalton Trans.* **2013**, *42*, 11941; b) A. Maurya, A. K. Mahato, N. Chaudhary, N. Kesharwani, P. Kachhap, V. K. Mishra, C. Haldar, *Appl. Organomet. Chem.* **2020**, 34.

[20] K. Dankhoff, M. Gold, L. Kober, F. Schmitt, L. Pfeifer, A. Dürrmann, H. Kostrhunova, M. Rothemund, V. Brabec, R. Schobert, B. Weber, *Dalton Trans.* **2019**, *48*, 15220.

[21] a) E. Monzani, L. Quinti, A. Perotti, L. Casella, M. Gullotti, L. Randaccio, S. Geremia, G. Nardin, P. Faleschini, G. Tabbı, *Inorg. Chem.* **1998**, *37*, 553; b) M. R. M. Quijano, G. F. Sueta, M. F. Álamo, N. A. Alcalde, V. G. Vidales, V. M. U. Saldívar, L. Gasque, *Dalton Trans.* **2012**, *41*, 4985.

[22] a) J. P. Donoso, C. J. Magon, J. F. Lima, O. R. Nascimento, E. Benavente, M. Moreno, G. Gonzalez, *J. Phys. Chem. C* **2013**, *117*, 24042; b) L. G. Sebastián, V. M. U. Saldívar, E. Mijangos, M. R. M. Quijano, L. O. Frade, L. Gasque, *J. Inorg. Biochem.* **2010**, *104*, 1112; c) S. Kumari, A. K. Mahato, A. Maurya, V. K. Singh, N. Kesharwani, P. Kachhap, I. O. Koshevoy, C. Haldar, *New J. Chem.* **2017**, 41; d) E. Faggi, R. Gavara, M. Bolte, L. Fajarí, L. Juliá, L. Rodríguez, I. Alfonso, *Dalton Trans.* **2015**, *44*(12), 700.

[23] a) V. K. Singh, A. Maurya, N. Kesharwani, P. Kachhap, S. Kumari, A. K. Mahato, V. K. Mishra, C. Haldar, *J. Coord. Chem.* **2018**, *71*(4), 520; b) M. R. Maurya, M. Bisht, A. Kumar, M. L. Kuznetsov, F. Avecilla, J. C. Pessoa, *Dalton Trans.* **2011**, *40*, 6968.

[24] M. Sutradhar, A. J. L. Pombeiro, *Reference Module in Chemistry, Molecular Sciences and Chemical Engineering*, Elsevier Inc **2017**.

[25] T. A. G. Duarte, A. P. Carvalho, L. M. D. R. S. Martins, *Catal. Sci. Technol.* **2018**, *8*, 2285.

[26] V. Conte, O. Bortolini, PATAI's Chemistry of Functional Groups, *Transition Metal Peroxides. Synthesis and Role in*

Oxidation Reactions, John Wiley & Sons, Ltd **2009**. https//doi.org/10.1002/9780470682531.pat0359.

[27] N. Mizuno, K. Kamata, *Coord. Chem. Rev.* **2011**, *255*, 2358.

[28] V. Conte, A. Coletti, B. Floris, G. Licini, C. Zonta, *Coord. Chem. Rev.* **2011**, 255.

[29] a) G. Romanowski, *J. Mol. Catal. A: Chem.* **2013**, *368*, 137; b) M. R. Maurya, M. Kumar, S. Sikarwar, *React. Funct. Polym.* **2006**, *66*, 808; c) M. R. Maurya, P. Saini, C. Haldar, A. K. Chandrakar, S. Chand, *J. Coord. Chem.* **2012**, *65*(16), 2903; d) G. Grivani, A. D. Khalaji, V. Tahmasebi, K. Gotoh, H. Ishida, *Polyhedron* **2012**, *31*(1), 265.

[30] V. Kogan, M. M. Quintal, R. Neumann, *Org. Lett.* **2005**, *7*(22), 5039.

[31] A. Nodzewska, A. Wadolowska, M. Watkinson, *Coord. Chem. Rev.* **2019**, *382*, 181.

[32] M. Sedighipoor, A. H. Kianfar, W. A. K. Mahmood, M. H. Azarian, *Inorg. Chim. Acta* **2017**, *457*, 116.

[33] B. Jarrais, A. Guedes, C. Freire, *New J. Chem.* **2018**, *42*, 2306.

[34] M. D. Hughes, Y. J. Xu, P. Jenkins, P. McMorn, P. Landon, D. I. Enache, A. F. Carley, G. A. Attard, G. J. Hutchings, F. King, E. H. Stitt, P. Johnston, K. Griffin, C. J. Kiely, *Nature* **2005**, *437*, 1132.

[35] M. Colladon, A. Scarso, P. Sgarbossa, R. A. Michelin, G. Strukul, *J. Am. Chem. Soc.* **2007**, *129*, 7680.

[36] N. Mizuno, Y. Nakagawa, K. Yamaguchi, *J. Mol. Catal. A: Chem.* **2006**, *251*, 286.

[37] M. C. Hsiao, S. T. Liu, *Catal. Lett.* **2010**, *139*, 61.

SUPPORTING INFORMATION

Additional supporting information may be found online in the Supporting Information section at the end of this article.

How to cite this article: Maurya A, Haldar C. Liquid-phase oxidation of olefins with rare hydronium ion salt of dinuclear dioxido-vanadium (V) complexes and comparative catalytic studies with analogous copper complexes. *Appl Organomet Chem*. 2021;e6203. https://doi.org/10.1002/aoc.6203